Charge Stoichiometry Inside Polyelectrolyte−Protein Complexes: A Direct SANS Measurement for the PSSNa−Lysozyme System

Jérémie Gummel,[†] François Boué,[†] Bruno Demé,[‡] and Fabrice Cousin*[,†]

Laboratoire Léon Brillouin, CEA Saclay, 91191 Gif sur Yvette Cedex, France, and Institut Laue Langevin, 6 rue Jules Horowitz, BP 156−38042 Grenoble Cedex 9, France

Received: July 12, 2006; In Final Form: September 21, 2006

We study by small angle neutron scattering and UV titration how the ratio of negative to positive charges, $[-]/[+]_{intro}$, acts on the structure of complexes formed by short negatively charged polyelectrolyte chains (PSS) and globular positively charged proteins (lysozyme). The range of $[-]/[+]_{intro}$ lies between 0.65 and 3.33. In all ratios, dense primary complexes are formed with radii around 10 nm. The species composition and the water content of the primary complexes are precisely obtained by the systematic use of the contrast matching of (deuterated) polymer or protein in SANS, yielding the compactness and the inner charge ratio $[-]/[+]_{inner}$. The primary complexes have (i) an inner charge ratio $[-]/[+]_{inner}$ close to 1 whatever $[-]/[+]_{intro}$, (ii) a high total volume fraction (0.25−0.4), (iii) a constant radius (75 Å) for $[-]/[+]_{intro} \leq 1$ that increases up to 150 Å for $[-]/[+]_{introduced} > 1$, and (iv) a shell of PSS chains when $[-]/[+]_{intro} > 1$. Moreover, UV titration shows that there are free proteins if $[-]/[+]_{introduced} < 1$ and free PSS chains if $[-]/[+]_{intro}$ is largely superior to 1. Hence, we observe that the primary complexes reach a finite size, controlled by electrostatic repulsion, and then aggregate at a higher scale with a fractal dimension of 2.1 characteristic of reaction-limited colloidal aggregation.

I. Introduction

Technological applications involving proteins and polyelectrolytes of opposite charges necessitate a fine control of the stability of the complexes they form. Keeping the complexes in solution is a key point in food or pharmacological industry, whereas tuning the degree of destabilization is indeed required for protein separation.[1−3] It is thus of fundamental interest to picture the structures of the complexes in order to understand the mechanisms driving their formation. A large amount of literature is now available (see, for example, refs 4 and 5).

Electrostatics is generally thought to be the relevant interaction in this formation (though hydrophobic interactions or hydrogen bonding are sometimes involved[6]). For example, when the protein charge density can be tuned by the pH (via the dissociation of amphoteric groups at the surface), the aggregation (followed by light scattering and turbimetry) is a maximum when the charges brought by the two components of the system are equal ($[-]/[+] = 1$). Complexation starts when polyelectrolytes interact with patches of opposite charge on the protein, even for a global charge of the same sign for protein and polyelectrolyte.[7,8] But at the corresponding critical pH_c, the size of the complexes is only some tens of nanometers, while it reaches much larger values at maximal aggregation.[9] In another work (BSA/PAH systems[10]), the reported behavior is similar. It is nevertheless not clear here whether the final growth proceeds by aggregation of the initial 10 nm objects or whether the inner structure of the complexes changes.

Concerning theory and simulations, many studies concern a system of a single macroion with a single chain,[11−13] while only a few simulations deal with several macroions associated with several chains.[14,15] These simulations show that adding some polyelectrolyte to a solution of macroions leads to the formation of soluble complexes. When the positive and negative charges introduced are equal ($[-]/[+]$ close to 1) and when the polyelectrolyte chains have a low persistence length (7−42 Å), the complexes are dense clusters that phase separate.[16] The complexes come back soluble when continuing to add polyelectrolyte. In this case, electrostatic interactions dominate the complexation process along with a counterion release. When the persistence length is higher (∼1500 Å), the solution of complexes stay monophasic whatever the charge ratio. The inhomogeneities of charge on the protein surface have also been taken into account in ref 15, where macroions are replaced by lysozyme. The formation of dense clusters for $[-]/[+]$ around 1 is also observed. The clusters are found with a "hairy" corona due to free chain ends, less complexed with proteins. Unfortunately, the numbers of proteins is limited to a few dozen in the simulation box, which keeps the aggregate size below the one observed in ref 9 or 10.

The counterion release is also proposed in calorimetric experiments made by Ball et al.,[10] who have shown that the complexation of BSA and PAH is endothermic and thus entropically favored. This can be due to the release of the counterions: the corresponding gained translation entropy counterbalances the loss of conformational entropy of the polymeric chains. Such a process has also been described on a DNA oligolysine system.[16,17] It is no doubt that we could take advantage of a structural picture of the complexation process: namely, the complexes size, compactness, and inner charges and the presence of an eventual polyelectrolyte brush at the surface of the complexes.

We propose to get this structural picture in accurate detail, using small angle neutron scattering (SANS), taking profit from

* Corresponding author. Phone: (33) 1 69 08 67 73. Fax: (33) 1 69 08 82 61. E-mail: fabrice.cousin@cea.fr.
[†] Laboratoire Léon Brillouin.
[‡] Institut Laue Langevin.

10.1021/jp064383k CCC: $33.50
Published on Web 11/15/2006

the contrast matching method. For that we extend a former work[18] on complexes made by lysozyme, a positively charged protein in acid buffer (pH 4.7, 5 10^{-2} mol/L acetate buffer), and sodium polystyrenesulfonate (PSSNa), a negatively charged polyelectrolyte. We let aside here our observations for the case ($[-]/[+] > 5$), where protein unfolds, which is specific of the lysozyme/PSSNa system. For lower charge excess ($3 < [-]/[+] < 5$), long chains form swollen gels where they are cross-linked by proteins. This suggests the role of the chain conformational entropy in limiting the formation of dense aggregates, as short chains mix with proteins into dense globular complexes (radius $\sim$ 10 nm) organized in a fractal way at a higher scale. In ref 18, the PSS chains are always in semidilute regime as their concentration is always higher than c^*, whatever the chain length. We suggest than the rolling of PSS chains around proteins induces a transition from the semidilute to the dilute regime for the shortest chains.

In this paper, we show that the short chain (50-repetition units)/lysozyme well-defined structure is ideal for a full characterization of the dense complexes that correspond to the dilute regime that is important for many industrial applications. As their c^* is rather high for the ionic strength we used (0.09 mol/L), they enable us to study samples with charge ratio $[-]/[+]$ close to 1 with high protein concentrations in the regime of the dense globular complexes. Deuteration of the chains, and use of D_2O/H_2O mixtures, takes full advantage of neutron radiation, which we combine with UV titration. First, we measure the exact size of the complexes and their compactness, which has never been done to our best knowledge. Second, we determine the localization of the different species (bounded in the core of the complexes, in a hairy shell around the complexes, or free in solution). That enables us to get the charge ratio within the complexes $[-]/[+]_{inner}$ and to compare it with the charge ratio introduced $[-]/[+]_{intro}$ in the solution. Finally, we get the structure factor of the complexes at larger scales, which gives a better picture of their aggregation mechanism. This allows us to picture the structure of the complexes for the different cases (Figure 8).

II. Materials and Methods

II.1. Sulfonation of Polystyrene. The synthesis of the sodium polystyrenesulfonate is done in several steps. We first purchase from Polymers Standard Service deuterated (for contrast matching in SANS studies) polystyrene chains of 50 repetition units ($M_w = 5000$), with a very low polydispersity ($M_w/M_n \sim 1.03$) A postsulfonation is then done on these chains in order to graft the sulfonate groups on the aromatic cycles. This reaction is done using Makowski's method.[19] A reactive species, created in-situ by the reaction between sulfuric acid and acetic anhydride, attacks the aromatic cycle, which grafts the sulfonate group in the para position (the ortho position is not grafted due to the chain steric hindrance). The poly(styrenic acid) solution is then neutralized by NaOH to obtain a PSSNa solution, eventually dialyzed against deionized water. The dialysis is followed by conductimetry and the water is renewed as many times as necessary to reach the conductivity of pure water. The solution is then concentrated in a rotating evaporator and finally freeze-dried to get a white powder that can be stored.

II.2. Samples Realization. Lysozyme is purchased from Sigma and used without further purification. All samples are done in an acetic acid/sodium acetate buffer solution to reach a pH of 4.7. The buffer concentration is set to have an ionic strength of 5 $\times$ 10^{-2} mol/L. Two solutions, one of lysozyme and one of PSSNa, are first prepared separately in the acetic buffer and then mixed and slightly shook to be homogenized. The samples are then left for 2 days at rest; we checked in previous experiments that this is enough to reach a stable state.

The studied $[-]/[+]_{intro}$ charge ratios are 0.65, 1, and 1.66, which are slightly inferior, equal, or superior to 1, and 3.33, which corresponds to the lowest charge ratio studied in our former work.[16] For that we always used a concentration of 40 g/L of protein (in order to get a good SANS signal) and the concentrations used for the PSSNa are 0.02, 0.03, 0.05, and 0.1 mol/L. For solutions of polyelectrolyte, c^* is equal to $1/(N_a N^{1/2} (2 l_p a)^{3/2})$, where N_a is the Avogadro number, N the number of repetitions units per chain, a the repetition unit length (2.05 Å[20]), and l_p the persistence length. For an ionic strength of 50 mM and the PSS concentrations considered, l_p lies around 50.[20] We get $c^* = 0.09$ mol/L, and only the sample at 0.01 mol/L is in the semidilute regime from the PSS chains point of view.

When mixture is achieved, a turbid fluid that strongly scatters light is instantaneously obtained for all the charge ratios. The different solutions have been revealed to remain macroscopically homogeneous over a period of 3 weeks. The charge ratio noted $[-]/[+]_{intro}$ is obtained as a function of the concentrations introduced, taking for the net charge of the lysozyme a value of +11 at pH 4.7) and for the charge of the PSSNa one negative charge per monomer. It corresponds to the ratio of the structural charges and not of the effective charges.

II.3. SANS Measurements. SANS measurements were done on the D22 spectrometer at the Institut Laue Langevin (Grenoble, France) in a q-range lying from 1 $\times$ 10^{-3} to 4 $\times$ 10^{-1} Å^{-1} and on the PAXY spectrometer at the Laboratoire Léon Brillouin (Saclay, France) in a q-range lying from 4 $\times$ 10^{-3} to 3 $\times$ 10^{-1} Å^{-1}. All measurements were done under atmospheric pressure and at room temperature.

To get either the PSSNa signal or the lysozyme signal independently, each PSS/protein composition was achieved in two solvents: once in a fully D_2O buffer that matches the neutron scattering length density of deuterated PSSNa and once in a 57%/43% H_2O/D_2O mixture that matches the neutron scattering length density of lysozyme.

Standard corrections for sample volume, neutron beam transmission, empty cell signal subtraction, and detector efficiency have been applied to get the scattered intensities on absolute scale for complexes samples [$I_{sample}(q)$] and for the pure buffers ($I_{buffer}(q)$, 100% D_2O or 57%/43% H_2O/D_2O). The scattering from the complexes $I_{complexes}(q)$ is obtained by subtracting from $I_{sample}(q)$ the solvent signal $I_{buffer}(q)$ and the incoherent calculated scattering from protons of lysozyme and PSSNA.

II.4. Ultraviolet Spectroscopy. UV spectroscopy measurements were done on a Varian Cary 100 UV−visible spectrometer. The λ range used is 240−340 nm. To separate complexes from free objects in solution (protein and polyelectrolyte) in the samples, we performed a centrifugation at 5000g. The supernatant, which was completely clear, was then poured into a UV quartz cell. The absorption in the UV range is due to the presence of absorbing chemical functions (aromatic) in the components, namely the benzenic cycle for PSSNa and tryptophan amino acid for the lysozyme, at characteristic absorption wavelengths. Concentration calibration has been done for solutions of protein alone, for the absorption maximum at a wavelength of 281 nm, and for solutions of polyelectrolyte alone at 261 nm. This allows a direct titration.

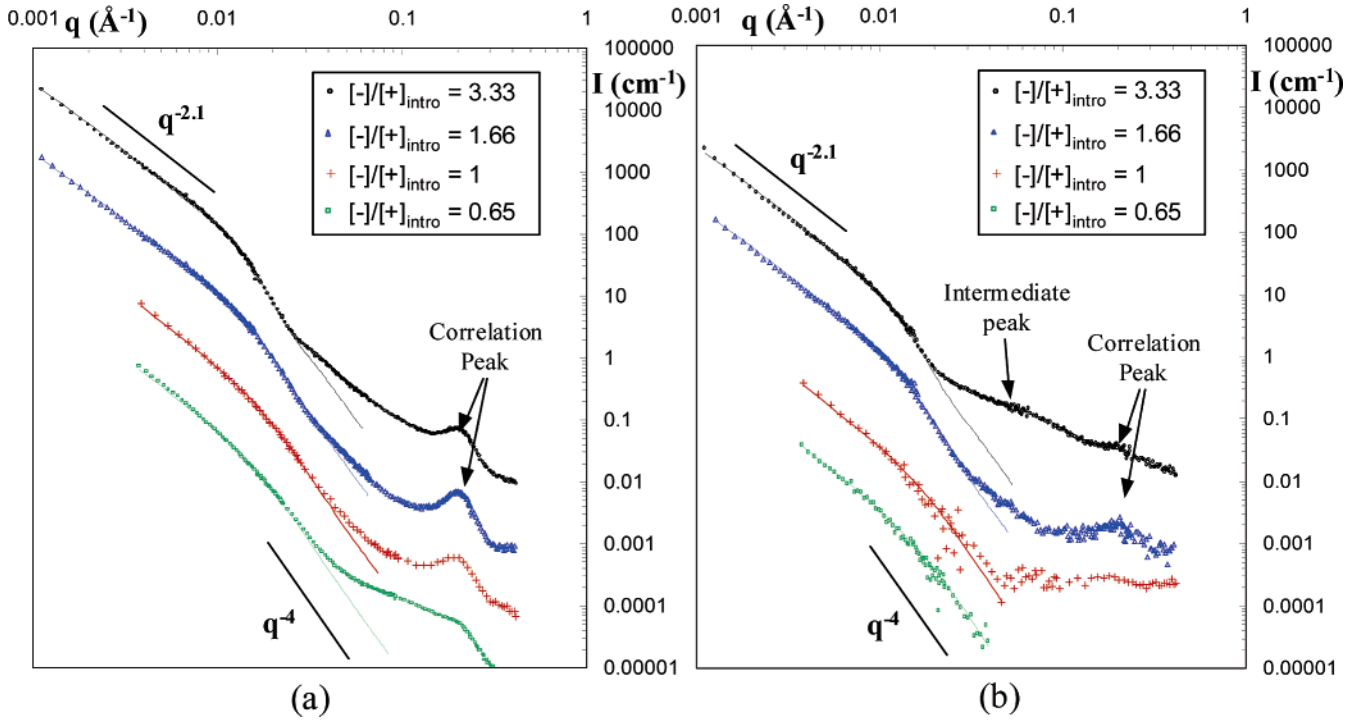

Figure 1. (a) Lysozyme scattering: black open circles, $[-]/[+]_{intro} = 3.33$; blue open triangles, $[-]/[+]_{intro} = 1.66$, the intensity is shifted (in the log−log plot) by a factor 0.1 to improve clarity; red crosses, $[-]/[+]_{intro} = 1$, the intensity is shifted by a factor 0.01 to improve clarity; green open squares, $[-]/[+]_{intro} = 0.65$, the intensity is shifted by a factor 0.001 to improve clarity; the full lines correspond to the fits presented in part IV. (b) PSS chains scattering: black open circles, $[-]/[+]_{intro} = 3.33$; blue open triangles, $[-]/[+]_{intro} = 1.66$, the intensity is shifted by a factor 0.1 to improve clarity; red crosses, $[-]/[+]_{intro} = 1$, the intensity is shifted by a factor 0.01 to improve clarity; green open squares, $[-]/[+]_{intro} = 0.65$, the intensity is shifted by a factor 0.001 to improve clarity; the full lines correspond to the fits presented in part IV.

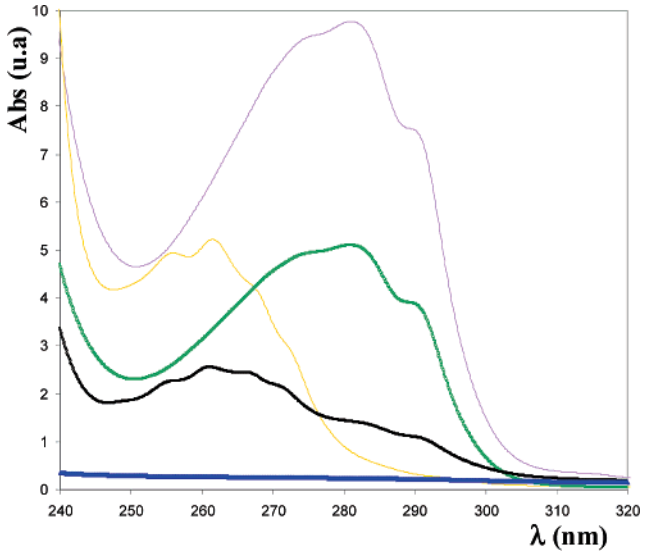

Figure 2. UV absorption spectra: purple continuous line, pure solution of lysozyme at 40 g/L; orange continuous line, pure solution of PSS chains (0.1 Mol/L); green open squares, $[-]/[+]_{intro} = 0.5$; blue open triangles, $[-]/[+]_{intro} = 1.66$ and $[-]/[+]_{intro} = 1$ (superimposed); black open circles $[-]/[+]_{intro} = 3.33$.

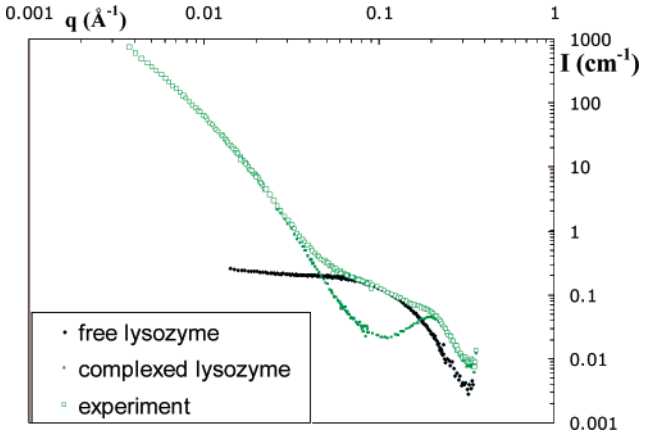

Figure 3. Scattering of lysozyme only for $[-]/[+]_{intro} = 0.65$ (PSS chains are matched): green open squares, total experimental signal; black filled diamonds, scattering of free lysozyme calculated from the form factor extracted from the signal of a 10 g/L dilute lysozyme solution and renormalized to the concentration of free lysozyme measured by UV titration; green filled squares, signal of complexes lysozyme after subtraction.

III. Results

III.1. SANS. The spectra are recorded 2 days after sample preparation. The SANS results for the four charge ratios are presented in Figure 1a for D_2O buffer (lysozyme scattering only) and Figure 1b for 57%/43% H_2O/D_2O buffer (PSS chains scattering only). The different q-ranges correspond respectively to measurements on D22 or on PAXY. The intensity of the spectra for $[-]/[+]_{intro} = 0.65$ in the 57%/43% H_2O/D_2O contrast is very weak due to the very low PSS content (0.02 mol/L) and does not allow us to get a significant signal at large q (after the subtraction of the incoherent background; hence, data are not plotted above ($q > 0.05$ Å^{-1}).

The protein scattering (in log−log plot) will be described first. For $[-]/[+]_{intro} = 1$, $[-]/[+]_{intro} = 1.66$, and for $[-]/[+]_{intro} = 3.33$, the spectra present the same features as we already observed in ref 18 for the same charge ratio with chains slightly longer (100 units; see Figure 3a).

At large q (0.2 Å$^{-1} < q < 0.4$ Å^{-1}), the intensity scatters as q^{-4}, as typical of the interface between solvent and a dense object. As seen in ref 18, the scattering in this q-range superimposes perfectly on the one of a diluted solution of

lysozyme only. It shows that the protein keeps its native globular conformation.

At 0.2 $Å^{-1}$ we see a strong correlation peak that corresponds to the contact of two proteins.

At intermediate q (from 0.2 to about 0.02 $Å^{-1}$), the intensity displays again the typical q^{-4} decay of dense objects. The proteins are thus densely packed at this scale to form the large 3D shaped primary complexes of several tenths of proteins.

Finally, for $q < 0.02$ $Å^{-1}$, there is a change of slope in the log−log plot, since the intensity scatters such as $q^{-2.1}$. The primary complexes are organized in a fractal way with a fractal dimension corresponding to the decay exponent. This 2.1 exponent differs from the one we previously reported (around 2.5) in ref 18. This is due to the fact that we estimated it on a small q-range where the scattering shifts from q^{-4} to $q^{-2.1}$. We have now extended the measurements toward low q and the fractal dimension is now estimated unambiguously on a q-range larger than a decade.

The only difference between the different spectra of Figure 1a lies in the intermediate q-range. The correlation hole at $q <$ 0.2 $Å^{-1}$ peak is deeper for both ratios 1 and 1.66, while the q range for the q^{-4} variation is shortened for ratio 3.33.

For $[-]/[+]_{intro} = 0.65$, the scattering is similar as the others charge ratios in the low q regime ($I \sim q^{-2.1}$) and intermediate q ($I \sim q^{-4}$) for $q < 0.05$ $Å^{-1}$ and for $q > 0.2$ $Å^{-1}$, where the scattering is only sensitive to the lysozyme form factor. It is different between 0.05 $Å^{-1} < q < 0.2$ $Å^{-1}$. It no longer shows a correlation peak but a bump at 0.2 $Å^{-1}$ and a shoulder at 0.1 $Å^{-1}$. This is due to some remaining free proteins in solution as we will show in part IV.1.1.

At large q all spectra superimpose on the protein signal at 40 g/L; hence, the protein scattering is perturbed neither by sedimentation nor by phase separation problems.

The polyelectrolyte scattering looks slightly different, but three features correspond exactly to the lysozyme one for all charge ratios: a peak at 0.2 $Å^{-1}$ (though more pronounced than for the protein), a q^{-4} behavior at intermediate q, and a $q^{-2.1}$ behavior at low q, both behaviors being very similar to the protein one in this low q range. The two components of the system are thus distributed in the same way in the complexes. The peak at 0.2 $Å^{-1}$ indicates that the polyelectrolyte chains are intermingled with proteins even at distances shorter than a diameter.

Despite the many common features between parts a and b of Figure 1, a single difference is striking, fully in the middle of the q range: for $[-]/[+]_{intro} = 3.33$ there is a maximum for q^* around 0.04−0.045 $Å^{-1}$. This is a reminder of the "polyelectrolyte peak", a signature of some remaining free chains in this sample (polyelectrolyte is here in large excess). This q^* is shifted toward low q compared to the value of a pure solution of PSS chains at the same concentration ($q^* = 0.057$ at 0.1 mol/L). As this maximum has completely disappeared for the other charge ratios, the concentration of free chains for the sample at $[-]/[+]_{intro} = 3.33$ is inferior to the whole concentration of chains introduced for $[-]/[+]_{intro} = 1.66$ (0.05 mol/L). The free chains are thus in dilute regime as c^* is 0.09 mol/L. As $q^* \propto c^{1/3}$ for pure solutions of polyelectrolyte chains in dilute regime and $q^* \propto c^{1/2}$ for semidilute regime,[21] the concentration of free chains that can be roughly estimated lies between 0.033 and 0.05 mol/L. The polyelectrolyte transient network initially present for $[-]/[+]_{intro} = 3.33$ has vanished. The structures obtained for the four charge ratios are thus very close though three samples are prepared in dilute regime and the fourth in semidilute regime.

TABLE 1: Free Species from UV Titration

	free lysozyme	free PSSNa
$[-]/[+]_{intro} = 0.65$	13 g/L (32.5%)	0
$[-]/[+]_{intro} = 1$	0	0
$[-]/[+]_{intro} = 1.6$	0	0.0015 M (3%)
$[-]/[+]_{intro} = 3.33$	4 g/L (10%)	0.04 M (40%)

III.2. Free Species Titration from UV Absorption. Figure 2 presents the UV spectra after centrifugation of samples for the four charge ratios, compared with the ones of pure solutions of lysozyme at 40 g/L and of PSSNa at 0.1 mol/L. All the fractions of free species are listed in Table 1. For $[-]/[+]_{intro} = 1.66$ and $[-]/[+]_{intro} = 1$, there are neither lysozyme nor PSS chains left in the supernatant: all species introduced into the solvent belong to the complexes. For the $[-]/[+]_{intro} = 0.65$, there remains an important fraction of free lysozyme but no PSS chains. Finally, for the ratio $[-]/[+]_{intro} = 3.33$, there remains an important part of free PSS chains and a few free lysozyme. The fraction of free PSS chains is in good accordance with the estimation from SANS scattering.

IV. Analysis of SANS Spectra

This analysis will start with the one lysozyme signal, which is more simple than the polyelectrolyte one. Indeed, as mentioned in the simulations of ref 15 and in our previous study,[18] it is possible that the complexes have a hairy shell of polymeric chains in addition to a core where protein and polyelectrolyte are both present. The PSSNa signal will thus be analyzed in the second place in section IV.2.

IV.1. Lysozyme Signal (D_2O Solvent). In this part the scattering of lysozyme at low q is modeled, considering that the low scattering is the scattering of dense globular complexes. In addition to the volume fraction of lysozyme introduced in the sample ϕ_{lyso}, three volume fractions have to be considered in this analysis: the volume fraction of the primary complexes Φ_{comp} (i.e. the volume occupied by all complexes divided by the sample volume), the volume fraction of lysozyme inside the primary complex Φ_{lyso_inner}, and the volume fraction (with respect to the whole volume of the sample) of the lysozyme present inside the complexes ϕ_{lyso_comp} (i.e., excluding proteins which do not belong to any complex). The latter is determined by UV titration.

IV.1.1. Subtraction of Signal of Free Lysozyme. For a better analysis of the scattering of complexes, the signal from free lysozyme can be subtracted from the total scattering, owing to our UV data. This is achieved by subtracting the signal of a pure dilute solution of lysozyme (proportional to its form factor), renormalized to the concentration of free lysozyme obtained from UV titration (see Table 1). The form factor has been measured on a pure solution of lysozyme at 10 g/L, which can be considered as diluted. Similarly, we assume that even for the highest concentration of free lysozyme founded on the complexes, 13 g/L for $[-]/[+]_{intro} = 0.65$, interactions between lysozyme are sufficiently weak to consider the free lysozyme in diluted regime. Figure 3 presents the spectra obtained for the $[-]/[+]_{intro} = 0.65$ after subtraction: we perfectly recover the features of the complexes signal obtained for the larger charge ratios: the $q^{-2.1}$ decay at low q, the q^{-4} decay at intermediate q, and the strong correlation peak at 0.2 $Å^{-1}$. This means that the differences before subtraction in the scattering for this charge ratio at intermediate q were only due to the presence of free lysozyme. The correlation peak at 0.2 $Å^{-1}$ was partially hidden by the lysozyme form factor, which resulted in a bump and also in a shoulder at 0.1 $Å^{-1}$. Note that for $q <$

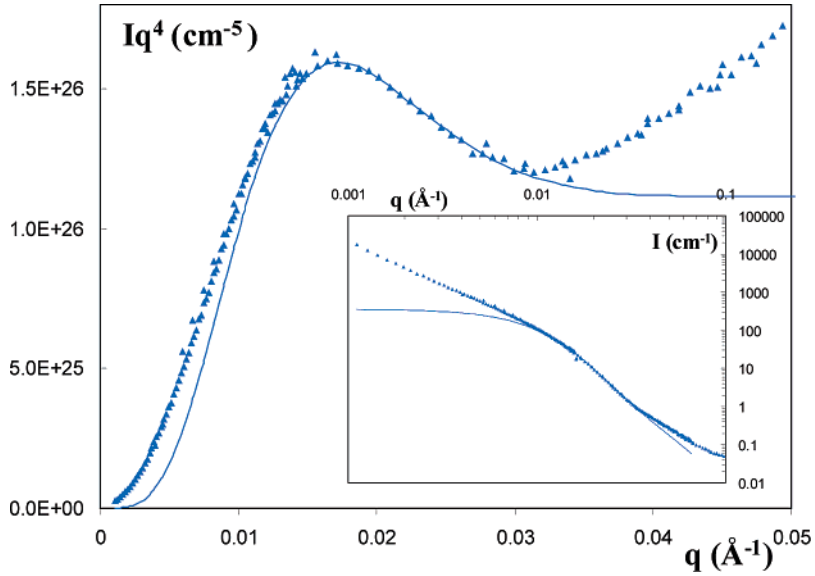

Figure 4. Blue triangles, lysozyme scattering for $[-]/[+]_{intro} = 1.66$ in a $I(q)q^4 = f(q)$ representation; blue continuous line, fit of the form factor of primary complexes corresponding to eqs 5−7. Inset: lysozyme scattering for $[-]/[+]_{intro} = 1.66$ and corresponding fit in log $I(q) = f(\log(q))$ representation.

0.05 Å^{-1}, the signal of the complexes is at least 10 times superior to that of the free lysozyme and several hundreds time higher for $q < 0.01$ Å^{-1}. The complexes signal is thus absolutely not affected by free lysozyme in this q-range.

IV.1.2. Size and Proteins Inner Volume Fraction of the Primary Complexes. Expression of the Scattering at Low q: The Effective Primary Complex Contrast. As explained in section III.1 and confirmed by the subtraction of free lysozyme, there are two q-ranges where the proteins scatter like q^{-4}, indicating the presence of objects with a well-defined interface at two length scales: the proteins seen as individual objects, at high q, and, at low q, what we will call the primary complexes containing proteins and chains densely packed. The threshold between those two regimes lies around 0.05 Å^{-1} and we can assume that beneath 0.03 Å^{-1} the scattering is only due to the complexes. This allows us to write

$$I_{lyso}(q)\ (cm^{-1}) = \Phi_{comp}\Delta\rho_{comp}{}^2 V_{comp}\, P_{comp}(q)\, S_{comp}(q) \quad \text{for } q < 0.03\ \text{Å}^{-1} \quad (1)$$

where Φ_{comp} is the volume fraction of the complexes, V_{comp} is their volume, $\Delta\rho_{comp}{}^2$ is the effective neutronic contrast between the complexes and the solvent, P_{comp} is their form factor, and S_{comp} is their structure factor.

Let us focus more on the term $\Delta\rho_{comp}{}^2$, which is the key point of our analysis. It is an effective neutronic contrast, i.e., the difference between the scattering length density of the solvent $\rho_{solvent}$ and the average scattering length density of the complex ρ_{comp}, since the latter can be considered as homogeneous at the scale of observation. The average composition of the complex comprises lysozyme with an inner volume fraction Φ_{lyso_inner}, solvent, and polyelectrolyte chains, which occupy together a volume fraction $(1 - \Phi_{lyso\_inner})$ and have here the same scattering length density, $\rho_{solvent}$. So we can write

$$\rho_{comp} = \Phi_{lyso\_inner}\rho_{lyso} + (1 - \Phi_{lyso\_inner})\rho_{solvent} \quad (2)$$

and the effective contrast between the complex and the solvent gets a very simple expression:

$$\Delta\rho_{comp}{}^2 = (\rho_{comp} - \rho_{solvent})^2 = \Phi_{lyso\_inner}{}^2(\rho_{lyso} - \rho_{solvent})^2 = \Phi_{lyso\_inner}{}^2\Delta\rho^2 \quad (3)$$

From UV titration we know the volume fraction of lysozyme in the sample that is involved in the complexes Φ_{lyso_comp}. The volume fraction of the complexes Φ_{comp} can be written as

$$\Phi_{comp} = \Phi_{lyso\_comp}/\Phi_{lyso\_inner} \quad (4)$$

Equation 1 can thus be rewritten like

$$I_{lyso}(q)\ (cm^{-1}) = \Phi_{lyso\_comp}\Phi_{lyso\_inner}\Delta\rho^2\, V_{comp}\, P_{comp}(q)\, S_{comp}(q) \quad (5)$$

Accessing the Primary Complex Form Factor. We can assume in a certain q-range, corresponding to the scale of an individual primary complex, that the scattering signal is only sensitive to the form factor; this occurs typically in the q-range where $I(q)$ scatters such as q^{-4}. Then

$$S_{comp}(q) \sim 1 \quad 0.01\ \text{Å}^{-1} < q < 0.03\ \text{Å}^{-1} \quad (6)$$

In a $I(q)q^4 = f(q)$ representation, a characteristic maximum appears in this q-range, as shown in Figure 4. This maximum is characteristic of the form factor of spherical objects and its position is linked to the average radius of the spheres. As there are no oscillations in the form factor, the size distribution of the complexes is polydisperse and we can assume that it follows a log-normal distribution

$$P(R) = \frac{1}{\sqrt{2\pi}\sigma R}\exp\left[-\frac{1}{2\sigma^2}\left(\ln\frac{R}{R_{comp}}\right)^2\right]$$

where R_{comp} is the most probable radius and σ the standard deviation. The mean volume of the primary complexes V_{comp_mean}, taking into account the polydispersity, is

$$V_{comp\_mean} = \frac{4\pi}{3}R_{comp}{}^3 e^{-9/2\sigma^2}$$

The experimental intensity of eq 5, with $S_{comp}(q) = 1$, can thus be perfectly fitted (see Figure 4) in the q-range domain lying

TABLE 2: Size, Proteins Inner Volume Fraction, and Mean Number of Proteins Involved in the Primary Complexes

	Φ_{lyso_inner}	R_{comp} (Å)	s	N_{lyso_comp}
$[-]/[+]_{intro} = 0.65$	0.24	73	0.45	65
$[-]/[+]_{intro} = 1$	0.19	73	0.45	53
$[-]/[+]_{intro} = 1.6$	0.27	114	0.37	214
$[-]/[+]_{intro} = 3.33$	0.3	154	0.31	485

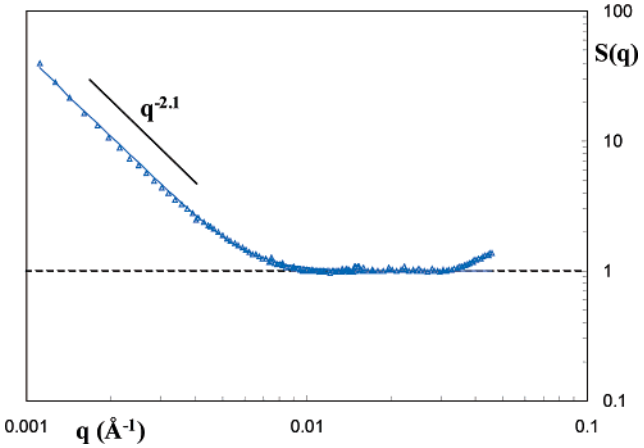

Figure 5. (b) Blue open triangles, structure factor for $[-]/[+]_{intro} = 1.66$ obtained by dividing the measured intensity by the form factor obtained from the fit of data (see Figure 4); continuous blue line, calculated structure factor of a fractal structure of polydisperse primary complexes with $D_f = 2.1$ (see the text).

from 0.01 and 0.03 Å^{-1} by using the average form factor of spheres:

$$V_{comp}P_{comp}(q) = \frac{\int_0^\infty \frac{4}{3}\pi R^3 \left(3\frac{\sin(qR) - qR\cos(qR)}{(qR)^3}\right)^2 R^3 P(R)\,dR}{\int_0^\infty R^3 P(R)\,dR} \quad (7)$$

The fit enables us to get both the form factor of $P_{comp}(q)$, namely the lysozyme inner volume fraction of the primary complexes Φ_{lyso_inner}, and the distribution parameter, the most probable radius R_{comp}, and the standard deviation σ. Results are listed in Table 2. Φ_{lyso_comp}, R_{comp}, and σ can be unambiguously determined, since they are locked to three different quantities in $I(q)$: R_{comp} is linked to the peak q-position, σ to the adjustment of the shape of the peak, and Φ_{lyso_comp} to the value of the intensity of the plateau after the peak in the $I(q)q^4 = f(q)$ representation. The sizes are the same for $[-]/[+]_{intro} = 0.65$ and $[-]/[+]_{intro} = 1$.

R_{comp} and Φ_{lyso_inner} enable us to get the mean number of lysozyme involved in a primary complex N_{lyso_comp}. This mean strongly increases with $[-]/[+]_{intro}$ as it shifts from a few dozen at $[-]/[+]_{intro} = 0.65$ to a few hundred at $[-]/[+]_{intro} = 3.33$.

IV.1.3. Structure Factor between Primary Complexes. The structure factor between the primary complexes (i.e. the spheres), $S_{comp}(q)$ is different from 1 at low q. In this q-range, it can be calculated from eq 5 by dividing the scattering intensity by the form factor of the complexes $P_{comp}(q)$ determined just above. $S_{comp}(q)$ is presented in Figure 5 for $[-]/[+]_{intro} = 1.66$. By principle, it is worth 1 between 0.01 and 0.03 Å^{-1}; at low q, it varies such as $q^{-2.1}$. This last exponent gives the fractal dimension D_f of the aggregates of primary complexes as it is well-known that $I(q)$ scatters such as q^{-D_f} for a fractal structure of dimension D_f.[22] Hence, we choose to model the structure factor simply like

$$S(q) = (q_c^{D_f})q^{-D_f} \quad \text{for } q < q_c \qquad S(q) = 1 \quad \text{for } q > q_c \quad (8)$$

where q_c is the cutoff wavevector for which the structure can be considered as fractal.

The value of q_c corresponds, for a given R_{comp}, to twice the diameter of the complexes ($q_c = 2\pi/4R_{comp}$), since a fractal structure cannot be defined on lower size ranges. Figure 5 presents the calculated structure factor with $D_f = 2.1$. The polydispersity of the complexes radius given in part IV.1.2 has been taken into account.

Finally, the whole scattering of the proteins can be modeled for $q < 0.03$ Å^{-1}; it is plotted as straight lines in Figure 1a for the different charge ratios.

The low q scattering of the structure factor enable to estimate a minimal value for the aggregation number N_{agg} of primary complexes in the large fractal structures formed at large scale. If such structures would have had a finite size smaller that the typical spatial scales probed at low q, the scattering would have reached a Guinier plateau at low q and the intensity would have tended toward N_{agg} times the form factor of complexes determined in eqs 6 and 7. The low q regime of the plateau is nevertheless never reached in the experiments, as the scattering still increases as $q^{-2.1}$ for the smallest q of the study. We get thus $N_{agg} > S(q_{min})$ that gives $N_{agg} > 40$ for $[-]/[+]_{intro} = 1.66$ and $N_{agg} > 42$ for $[-]/[+]_{intro} = 3.33$, the two samples studied at the lowest q. The large fractal structure formed by the primary dense complexes are thus made by at least several tens of complexes.

IV.2. PSS Chains Signal (D_2O/H_2O Solvent). *IV.2.1. Checking for the Presence of a Polymeric Shell.* As stated in section III.1, both the scattering of proteins in a 100% D_2O buffer and polymeric chains in a 57%/43% H_2O/D_2O buffer present the same global features at low q, indicating that the two kinds of objects are roughly organized in the same way in the complexes. The primary complexes display mostly the same shape and their fractal organization looks the same, from the point of view of the PSS chains or from the point of view of the lysozyme.

We can check that in more detail. Following eqs 1−4, at the scale of primary complexes, the PSS scattering is expressed exactly like the lysozyme scattering, i.e., as eq 1. The terms Φ_{comp} and V_{comp} are the same as in the lysozyme scattering. $(\rho_{PSS} - \rho_{solvent})^2$ in the 57%/43% H_2O/D_2O buffer is equal to $(\rho_{lyso} - \rho_{solvent})^2$ in the 100% D_2O buffer for symmetrical reasons

$$\Delta\rho_{comp}{}^2 = \Phi_{PSS\_inner}{}^2 \Delta\rho^2 \text{ (polyelectrolyte signal)} \quad (9)$$

where Φ_{PSS_inner} is the volume fraction of PSS chains within the complex.

If we assume that $P_{comp}(q)$ and $S_{comp}(q)$ are the same when we look at lysozyme and at PSS, we can write at low q:

$$I_{PSS}(q)/I_{lyso}(q) = (\Phi_{PSS\_inner}/\Phi_{lyso\_inner})^2 \quad (10)$$

If this is true, the ratio between the intensities of the lysozyme scattering and the PSS scattering should thus be constant in the low q regime. On the contrary, if the primary complexes have a polymeric shell, their effective size is higher from the point of view of the PSS chains than from the point of view of lysozyme. $P_{comp}(q)$ would be different for PSS. This would extend the q-range where $I_{PSS}(q)$ scatters such as q^{-4} to lower q and $I_{PSS}(q)/I_{lyso}(q)$ would monotonically increase when q tends

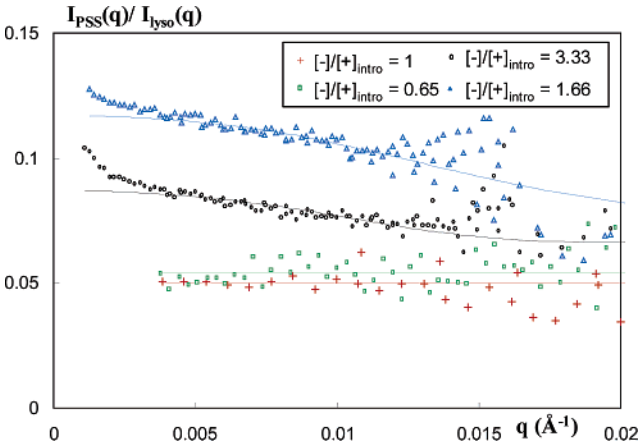

Figure 6. $I_{PSS}(q)/I_{lyso}(q)$ at low q: black open circles, $[-]/[+]_{intro} = 3.33$; blue open triangles, $[-]/[+]_{intro} = 1.66$; red crosses, $[-]/[+]_{intro} = 1$; green open squares, $[-]/[+]_{intro} = 0.65$. The black and blue continuous lines correspond to the fits described in part IV.2.3 for $[-]/[+]_{intro} = 3.33$ and $[-]/[+]_{intro} = 1.66$. The green line is a constant equal to 0.055. The red line is a constant equal to 0.05.

toward 0. Figure 6 presents $I_{PSS}(q)/I_{lyso}(q)$ for the four charge ratios at low q. $I_{PSS}(q)/I_{lyso}(q)$ is constant only for $[-]/[+]_{intro} = 0.65$ and $[-]/[+]_{intro} = 1$. For $[-]/[+]_{intro} > 1$, $I_{PSS}(q)/I_{lyso}(q)$ increases, indicating that there is a polymeric shell when negative charges are introduced in excess.

We will now discuss separately the case of complexes without polymeric shell and with polymeric shell.

IV.2.2. Inner Charge Ratio and Compactness of Complexes without Polymeric Shell. When $I_{PSS}(q)/I_{lyso}(q)$ is constant, its value provides a direct access to the ratio of species within the complexes $\Phi_{PSS\_inner}/\Phi_{lyso\_inner}$ and thus to the inner charge ratio $[-]/[+]_{inner}$. Please note that in this case the inner charge ratio can be obtained without any fitting of the scattering. We get, for $[-]/[+]_{intro} = 0.65$, $I_{PSS}(q)/I_{lyso}(q) = 0.055$, i.e. $\Phi_{PSS\_inner}/\Phi_{lyso\_inner} = 0.23$ and $[-]/[+]_{inner} = 0.97$. For $[-]/[+]_{intro} = 1$, we get $I_{PSS}(q)/I_{lyso}(q) = 0.05$, i.e. $\Phi_{PSS\_inner}/\Phi_{lyso\_inner} = 0.22$ and $[-]/[+]_{inner} = 0.91$.

The inner charge ratios $[-]/[+]_{inner}$ are thus very similar, though the introduced charge ratios are different. Moreover, they are very close to 1.

$I_{PSS}(q)/I_{lyso}(q)$ also allows us to get the compactness of the primary complexes Φ_{inner}:

$$\Phi_{inner} = \Phi_{PSS\_inner} + \Phi_{lyso\_inner} = \Phi_{lyso\_inner}\,(1 + I_{PSS}/I_{lyso}^{1/2}) \quad (11)$$

$$\Phi_{inner} = 0.3 \quad \text{for } [-]/[+]_{intro} = 0.65$$

$$\Phi_{inner} = 0.24 \quad \text{for } [-]/[+]_{intro} = 1$$

The primary complexes have a very high density.

Knowing Φ_{PSS_inner}, it is also possible to determine from the scattering the volume fraction of PSS chains involved in the complexes, noted as Φ_{PSS_comp}. We write the PSS scattering as

$$I_{PSS}(q)\ (\text{cm}^{-1}) = \Phi_{PSS\_comp}\Phi_{PSS\_inner}\,\Delta\rho^{2}V_{comp}\,P_{comp}(q)\,S_{comp}(q) \quad \text{for } q < 0.03\ \text{Å}^{-1} \quad (12)$$

Dividing Φ_{PSS_comp} by the quantity introduced in the sample, we finally get the ratio of PSS chains involved in complexes $r_{PSS\_comp} \sim 1$. We can now compare the results with those from our UV titration (see Table 1) and find a good agreement. All values are listed in Tables 3 and 4.

TABLE 3: Size and PSS Chains Inner Volume Fraction of the Core and the Shell of the Primary Complexes

	r_{PSS_comp}	Φ_{PSS_inner}	$R_{comp\_coreshell}$ (Å)	σ
$[-]/[+]_{intro} = 0.65$	~1	0.052	73	0.45
$[-]/[+]_{intro} = 1$	~1	0.041	73	0.45
$[-]/[+]_{intro} = 1.66$	~1	0.069	154	0.35
$[-]/[+]_{intro} = 3.33$	0.43	0.075	164	0.31

TABLE 4: Inner Volume Fraction and Inner Charge Ratio of the Primary Complexes

	$\Phi_{PSS\_inner}/\Phi_{lyso\_inner}$	Φ_{inner}	$[-]/[+]_{inner}$
$[-]/[+]_{intro} = 0.65$	0.235	0.29	0.97
$[-]/[+]_{intro} = 1$	0.22	0.24	0.91
$[-]/[+]_{intro} = 1.66$	0.25	0.34	1.03
$[-]/[+]_{intro} = 3.33$	0.25	0.375	1.03

IV.2.3. Complexes with a Polymeric Shell. When there is a polymeric shell, the form factor of the primary complexes is, from the PSS chains point of view, a core−shell structure with a core radius R_{core} equal to the radius R_{comp} deduced from the lysozyme scattering. The polymeric shell is necessary thin since (i) we use chains with $N = 50$ and (ii) each chain that belongs to the shell has a part buried within the core. At the surface of the core, the density of the anchored PSS chains is equal to the density of the chains within the primary complexes. Since the shell is thin, this density cannot change much, so we can assess that the inner volume fraction of the PSS chains is similar within the core and within the shell. Since one sees the chains, the core−shell structure appears as homogeneous; it can be described again by spheres, with a new mean diameter $R_{comp\_coreshell}$ and a new polydispersity $\sigma_{comp\_coreshell}$. This last polydispersity is very close to that of the core because $R_{comp\_coreshell} - R_{comp}$ (the thickness) is small. For the same reason, the structure factor $S_{comp}(q)$ is close to the one obtained in the lysozyme scattering. As the free chains scattering is negligible at low q, the total scattering is written as

$$I_{PSS}(q)\ (\text{cm}^{-1}) = \Phi_{comp\_coreshell}\Phi_{PSS\_inner}^{2}(\rho_{PSS} - \rho_{solvent})^{2}V_{comp\_coreshell}\,P_{comp\_coreshell}(q)\,S_{comp}(q) \quad (13)$$

where $\Phi_{comp\_coreshell}$ is the volume fraction of the complexes with a core−shell structure from the PSS scattering point of view, $V_{comp\_coreshell}$ is their volume, and $P_{comp\_coreshell}$ their form factor.

To point out the differences of radii between the core of the primary complexes (lysozyme scattering) and the core−shell structure (PSS scattering), we have divided both the lysozyme scattering and the PSS scattering by the structure factor $S_{comp}(q)$ obtained in section IV.1.3 to focus on their form factor. All the different form factors are presented, in $q^4P(q)$ representation, in Figure 7. All curves present a maximum characteristic of their radius size. It clearly appears that the maximum is shifted toward lower q, i.e. larger size, when passing from the lysozyme scattering to the PSS scattering. The values of $R_{comp\_coreshell}$ and $\sigma_{comp_}$coreshell, obtained from the fits of the form factors of polydisperse spheres, plotted as solid lines in Figure 7, are listed in Table 3, to compare with the values in Table 2 for lysozyme scattering.

The values of $\Phi_{comp\_coreshell}\Phi_{PSS\_inner}^{2}$ can be deduced from fits of Figure 7. $\Phi_{comp\_coreshell}$ is linked to the complexes volume fraction in the lysozyme case Φ_{comp}, which is reported in part IV.1.2, by the relation

$$\Phi_{comp\_coreshell} = \Phi_{comp}(V_{comp\_coreshell\_mean}/V_{comp\_mean})^{3} \quad (14)$$

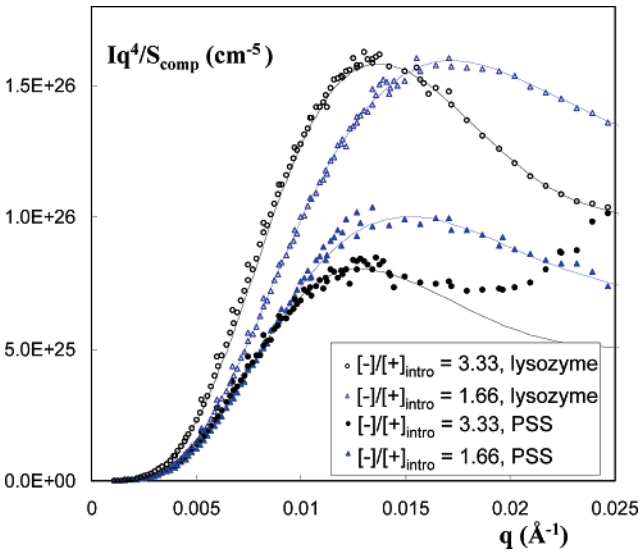

Figure 7. Form factors of primary complexes: black open circles, $[-]/[+]_{intro} = 3.33$, lysozyme scattering; black filled circles, $[-]/[+]_{intro} = 3.33$, PSS scattering (the PSS scattering intensity is magnified by a factor 7 to improve clarity); blue open triangles, $[-]/[+]_{intro} = 1.66$, lysozyme scattering; blue filled triangles, $[-]/[+]_{intro} = 1.66$, PSS scattering (the PSS scattering intensity is magnified by a factor 7 to improve clarity). The continuous lines correspond to fits of polydisperse spheres. The parameters values are listed in Tables 2 and 3.

It is finally possible to obtain the PSS inner volume fraction Φ_{PSS_inner} in the core−shell structure. Values are listed in Table 3.

The volume fraction of PSS chains, Φ_{PSS_comp}, involved in the complexes can also be obtained, since

$$\Phi_{comp\_coreshell} = \Phi_{PSS\_comp}/\Phi_{PSS\_inner} \qquad (15)$$

This yields the ratio of chains involved in the complexes r_{PSS_comp}. It is equal to 1 for $[-]/[+]_{intro} = 1.66$, in accordance with the UV titration measurements, but is ~0.43 for $[-]/[+]_{intro} = 3.33$, though we get 0.6 from UV titration.

Finally, the whole scattering of the PSS chains can be modeled for $q < 0.03$ Å^{-1} and is plotted as solid lines in Figure 1b for the different charge ratios.

IV.3. Inner Volume Fraction and Inner Charge Ratio of the Primary Complexes. Finally, the above-reported measurements of Φ_{PSS_inner} and Φ_{lyso_inner} enable us to get the inner volume charge ratio $[-]/[+]_{inner}$ and the complexes inner volume fraction Φ_{lyso_inner}. All values are recalled in Table 4.

Though the values of $I_{PSS}(q)/I_{lyso}(q)(q\rightarrow 0)$, which are a direct measurement of $\Phi_{PSS\_inner}/\Phi_{lyso\_inner}$ when primary complexes have no polymer shell, are very different from one sample to another (see Figure 6), the final values of $\Phi_{PSS\_inner}/\Phi_{lyso\_inner}$ are very close for all samples. The large discrepancies of $I_{PSS}(q)/I_{lyso}(q)(q\rightarrow 0)$ are due to the presence of the polymeric shell. The increase of the effective primary complex radius by the presence of the polymer shell, when PSS is seen, strongly enhances $I_{PSS}(q)/I_{lyso}(q)(q\rightarrow 0)$.

Moreover, as the polymer shell keeps a constant size (related to the chain length), the relative increase of the primary complexes volume, when passing from lysozyme to PSS, decreases when R_{comp} increases. Hence, $I_{PSS}(q)/I_{lyso}(q)(q\rightarrow 0)$ decreases when R_{comp} increases (compare $I_{PSS}(q)/I_{lyso}(q)$ for $[-]/[+]_{intro} = 1.66$ and $[-]/[+]_{intro} = 3.33$).

Finally, the calculation of $I_{PSS}(q)/I_{lyso}(q)$ from the different radii and inner volume fractions fits perfectly the experimental value (see Figure 6), except at very low q. At such low q, we see an excess of PSS scattering, mostly for $[-]/[+]_{intro} = 3.33$. This upturn is thus probably due to aggregates of free PSS chains, as classically observed on pure solutions of PSS chains.[23]

V. Discussion

In Figure 8is shown a picture of the structures formed as they are deducted from SANS experiments. In addition, the main features of the different cases observed are recalled: (1) they have a high compactness (between 0.25 and 0.4); (2) their inner charge ratio $[-]/[+]_{inner}$ is constant (~ 1, whatever $[-]/[+]_{intro}$; (3) the radius of the primary complexes R_{comp} is constant for $[-]/[+]_{intro} \leq 1$ and increases with $[-]/[+]_{intro}$ for $[-]/[+]_{intro} > 1$; (4) the mean number of proteins involved in primary complexes increases from a few dozen for $[-]/[+]_{intro} \leq 1$ to a few hundred for $[-]/[+]_{intro} = 3.33$; (5) there is a polymeric shell if $[-]/[+]_{intro} > 1$; (6) there are free proteins but no polymeric shell if $[-]/[+]_{intro} < 1$ and free polyelectrolyte chains if $[-]/[+]_{intro}$ is largely superior to 1; (7) the primary complexes are organized in a fractal way with a fractal dimension $D_f = 2.1$ at large scale. The aggregation number N_{agg} is superior to a few dozen primary complexes.

In our previous paper,[18] we showed that there are two characteristics times in the system. A first one, fast, where the primary complexes are formed, and a second one, long, where those complexes aggregate at a larger scale. We discuss thus here first the influence of the introduced charge ratio $[-]/[+]_{intro}$ on the formation of the primary complexes and second the mechanism of their further aggregation.

V.1. Formation of the Primary Complexes. First of all please note that the main structures of the primary complexes (dense 3D-objects with a finite size) are obtained in the range of introduced charge ratios $[-]/[+]_{intro}$ which has a large intersection with the one of our former study.[18] The process of complexes formation is thus similar to the one we describe in ref 18. Direct electrostatic interactions between lysozyme and PSS chains lead to the contraction of the polymeric chains around the proteins. For small chains such as the ones studied here and in a part of our former paper, the transient network formed by PSS chains initially present in semidilute regime is destroyed by the chain contraction during the formation of dense primary complexes. We confirm here this mechanism as we get exactly the same kind of structure if the PSS chains are initially in dilute regime. In our former work, we also studied the case of long polyelectrolyte chains, which keep the system in semidilute regime and leads to gel formation. This is not the case here. Also, the present study does not consider the case of lysozyme unfolding, which occurs for higher $[-]/[+]_{intro}$.

The present study enables us to refine the process of the structure formation. As the inner charge ratio $[-]/[+]_{inner}$ in the core of the complex stays close to 1, whatever $[-]/[+]_{introduced}$ (see Table 4 and Figure 9), the complexation appears to be electrostatically stoichiometric, as seen in simulations.[14,15] This is different from the case of complexation involving PSS chains and β-lactoglobulin, which is not stoichiometric,[24] but in this last case the two species bear the same charge and interact by the patch charges.

As the complexation is stoichiometric, all species introduced in excess from an electrostatic point of view remain in solution outside of the core of the primary complexes (see the concentration of free species in Tables 1 and 3). In the case of a slight excess of negative charges, some PSS chains, which can partly belong to the core of the complexes, will form a polymeric shell around the complexes.

As the observed complexation process involves a stoichiometry of 1, all the structural negative charges are accessible to

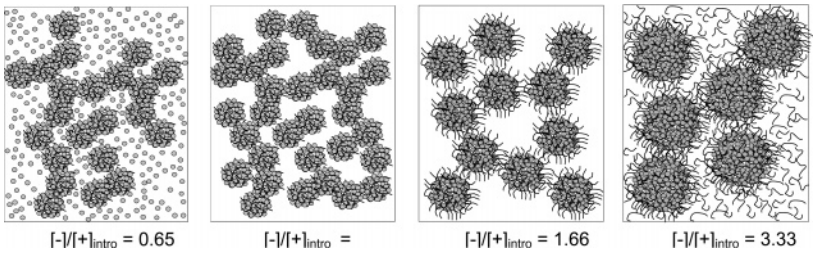

Figure 8. Pictures of the different structures of lysozyme−PSSNa complexes as suggested by SANS when $[-]/[+]_{intro}$ is close to 1.

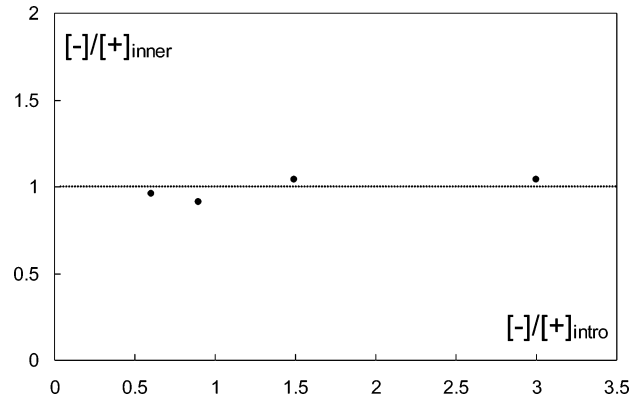

Figure 9. Inner volume fraction of the complexes.

the positive charges of the proteins. All the counterions are thus released from the PSS chains. It is very likely that the counterions released far from the chains will be released out of the primary complexes, because they are highly compact and the process is entropically favorable. The complexation is thus driven by the enthalpic gain due to electrostatic interactions plus the entropic gain due to release of counterions that compensate the loss of entropy of polymeric chains, as suggested in refs 10 and 16.

It still remains unclear why the formation of primary complexes stops at such a well-defined size. Our results nevertheless allow us to point out some parameters that govern the size of the primary complexes. First, for $[-]/[+]_{intro}$ varying between 0.65 and 1, the complexes have the same size (around 75 Å) and quite the same mean number of proteins per complex (50−60). Since there are more proteins involved in the complexes for 1 than for 0.65, this implies that the number of complexes increases. We can see this effect as the fact that the number of nucleation sites for a primary complex increases proportionally to the protein concentration. Second, when $[-]/[+]_{intro} > 1$, the mean number of proteins per complex now strongly increases when $[-]/[+]_{intro}$ increases: from 60 for 1 up to ∼200 for 1.66 and ∼500 for 3.33. It therefore seems that an excess of polyelectrolyte generates more configurations where proteins and PSS chains can electrostatically interact. The increase in ionic strength brought by the added polyelectrolyte with an increase of $[-]/[+]_{intro}$ can also play a role in the final value of N_{lyso_comp}. When proteins and PSS chains start to interact, they progressively form small aggregates of N_{lyso_comp} that are charged on surface (slightly positively when $[-]/[+]_{intro} < 1$ or slightly negatively when $[-]/[+]_{intro} > 1$). The global charge Z_{comp} is thus linked to the objects present at the complexes surface and increases as $N_{lyso\_comp}^{2/3}$. The fast aggregation stops thus when the electrostatic repulsion between aggregates is sufficiently high to stabilize the system to form the primary complexes. As the electrostatic interaction is strongly screened by the ionic strength following DLVO theory,[25] this aggregation arrest occurs at high N_{lyso_comp} for high salinity. Z_{comp} should be indeed quite similar from one sample to another for a given N_{lyso_comp}.

V.2. Aggregation of the Primary Complexes. Once the primary complexes are formed, they still interact, since we observe aggregates at a higher scale. The fractal dimension of such aggregates of primary complexes is 2.1. This fractal dimension is characteristic of a reaction-limited colloidal aggregation (RLCA) process,[26] as found both in simulations and experiments.[27−29] Such an aggregation is dominated by the chemical (or physicochemical) reaction time between objects, a process that generally occurs for charged systems. It is the opposite of diffusion-limited colloidal aggregation (DLCA), where the aggregation is driven only by the diffusion of the objects and leads to the formation of objects with a lower fractal dimension (1.78).[30]

The primary complexes bear charges on their surface (negative when $[-]/[+]_{intro} > 1$ and positive charged when $[-]/[+]_{intro} < 1$) as they are stabilized by electrostatic repulsions. There should nevertheless also remain some positive charges on negatively charged complexes and some negative charges on positively charged complexes to induce the aggregation, otherwise electrostatic repulsions between primary complexes should completely stabilize the system. For $[-]/[+]_{intro} = 1$, the surface of the primary complexes should be globally neutral. One thus may expect the aggregation process of primary complexes to turn to DLCA, which we did not observe. Another process we can think of is phase separation, as suggested in ref 14: because the primary complexes now have high masses, their charge may not be enough for the suspension to be stable. This could lead to droplets of a concentrated phase, inducing the formation of a fractal.

Whatever the sample studied, the regime where the $q^{-2.1}$ scattering of the aggregates reaches a plateau is never reached in the smallest q of our study (10^{-3}), which should occur at $q_c = 2\pi/4R_{comp}N_{agg}^{1/D_f}$ in the case of aggregate size. The aggregates have a minimal aggregation number N_{agg} superior to 40 and thus a size higher than 3000 Å, i.e. higher than 10 primary complexes diameters. We were not able to measure the size of those aggregates, as they are out of the neutron scale range and as the solutions are too concentrated to perform light scattering on them. A good way to determine their size would be to dilute the solution a posteriori to keep the structure formed, but it will be impossible to know if we would not be changing the size of the aggregates.

VI. Conclusion

We have determined here the structure of complexes formed by small polyelectrolyte chains (PSS) and proteins (lysozyme) of opposite charges with small angle neutron scattering. We have especially studied the influence of the ratio of positive and negative charges introduced in the solution $[-]/[+]_{intro}$ in a range where this ratio is close to a stoichiometry of 1 ($0.65 < [-]/[+]_{intro} < 3.33$). The complexes have very close structures, whenever the PSS chains are initially in dilute or

semidilute regime. They form 3-D primary complexes with a radius lying from 75 Å for the lowest $[-]/[+]_{introduced}$ to 150 Å for the highest $[-]/[+]_{introduced}$. Such primary complexes are organized at a higher scale in aggregates of fractal dimension 2.1.

Besides the determination of the different characteristic scales of the systems, the systematic use of the contrast matching method for both the protein scattering and the polyelectrolyte scattering has allowed us to measure the species composition and the water content within the core of the solvated complexes, and thus their compactness and their inner charge ratio $[-]/[+]_{inner}$. This is to our best knowledge the first time that such kind of information is obtained on solvated complexes. This successful method can be applied to any system involving two components in a solvent, as soon as there is a sufficiently high difference of neutron density lengths between the two components of the system (such a difference can generally be obtained by deuterium labeling).

The primary complexes have a very high density (their inner volume fraction lies between 0.25 and 0.4) and their inner charge ratio $[-]/[+]_{inner}$ stays always close to 1, whatever $[-]/[+]_{intro}$. The process of the complexation is thus purely stoichiometric from an electrostatic point of view. All the species introduced in excess do not participate in the complexation. The proteins in excess remain in solution when $[-]/[+]_{intro} < 1$. The PSS chains remain either in a shell surrounding the primary complexes or in solution when $[-]/[+]_{intro} > 1$. Both the high compactness of the primary complexes and the constant value of $[-]/[+]_{inner}$ equal to 1 suggests a release of the counterions from the inner of the primary complexes. The complexation is thus driven by the electrostatic interactions and favored by a gain of entropy due to release of counterions. The increase of the radius of primary complexes with the increase of salinity when adding polyelectrolyte suggests that the finite size of primary complexes is due to electrostatic repulsions between primary complexes.

Once the primary complexes are formed, they still interact to form aggregates at a higher scale. The fractal dimension of the aggregates (2.1) is characteristic of a reaction-limited colloidal aggregation process, which generally occurs for charged systems.

The stoichiometric, electrostatically driven complexation may be affected by large modifications of the interactions in the system. We plan to consider these effects in forthcoming studies and try to clear up a remaining question: why does electrostatic complexation lead to primary complexes of finite size?

References and Notes

(1) Morawetz, H.; Hughes, W. L. *J. Phys. Chem.* **1951**, *56*, 64−69.

(2) Mattison, K. W.; Brittain, I. J.; Dubin, P. L. *Biotechnol. Prog.* **1995**, *11* (6), 632−637.

(3) Wang, Y.; Gao, J. Y.; Dubin, P. L. *Biotechnol. Prog.* **1996**, *12* (3), 356−362.

(4) Cooper, C. L.; Dubin, P. L.; Kayitmazer, A. B.; Turksen, S. *Curr. Opin. Colloid Interface Sci.* **2005**, *10*, 52−78.

(5) Doublier, J. L.; Garnier, C.; Renard, D.; Sanchez, C. *Curr. Opin. Colloid Interface Sci.* **2002**, *5*, 202−214.

(6) Tribet, C. *Complexation between amphiphilic polyelectrolytes and proteins*: *From necklaces to gels;* Surfactant Science Series "Physical chemistry of polyelectrolytes"; Radeva, T., Ed.; Dekker: New York, 1999; Chapter 19, pp 687−741.

(7) Park, J. M.; Muhoberac, B. B.; Dubin, P. L.; Xia, J. *Macromolecules* **1992**, *25*, 290−295.

(8) Tsuboi, A.; Izumi, T.; Hirata, M.; Xia, J.; Dubin, P. L.; Kokufuta, E. *Langmuir* **1996**, *12*, 6295−6303.

(9) Xia, J.; Dubin, P. L.; Kim, Y.; Yesook; Muhoberac, B. B.; Klimkowski, V. J.; Valentine, J. *J. Phys. Chem.* **1993**, *97*, *7* (17), 4528−4534.

(10) Ball, V.; Winterhalter, M.; Schwinte, P.; Lavalle, Ph.; Voegel, J.-C.; Schaaf, P. *J. Phys. Chem. B*, **2002**, *106*, 2357−2364.

(11) Netz, R.; Joanny, J. F. *Macromolecules* **1999**, *32*, 9026−9040.

(12) Chodanowski, P.; Stoll, S. *J. Chem. Phys.* **2001**, *115* (10), 4951−4960.

(13) Stoll, S.; Chodanowski, P. *Macromolecules* **2002**, *35*, 9556−9562.

(14) Skepö, M.; Linse, P. *Macromolecules* **2003**, *36*, 508−519.

(15) Carlsson, F.; Linse, P.; Malmsten, M. *J. Am. Chem. Soc.* **2003**, *125*, 3140−3149.

(16) Mascotti, D. P.; Lohman, T. M. *Biochemistry* **1993**, *32*, 10568−10579.

(17) Mascotti, D. P.; Lohman, T. M. *Biochemistry* **1993**, *31*, 8932−8946.

(18) Cousin, F.; Gummel, J.; Ung, D.; Boué, F. *Langmuir* **2005**, *21*, 9675−9688.

(19) Makowski, H. S.; Lundberg, R. D.; Singhal, G. S. (EXXON Research and Engineering Co.) US Patent 3 870 841, 1975.

(20) Spiteri, M. N.; Boué, F.; Lapp, A.; Cotton, J. P. *Phys. Rev. Lett.* **1996**, *77*, 5218−5220.

(21) Williams, C.; Nierlich, M.; Cotton, J. P.; Jannink, G.; Boué, F.; Daoud, M.; Farnoux, B.; Picot, C.; de Gennes, P. G.; Rinaudo, M.; Moan, M.; Wolff, C. *J. Polym. Sci., Polym. Lett. Ed.* **1979**, *17*, 381.

(22) Cabane, B. Growth: A brief guide for the use of scattering techniques. In *Neutron, X.-Ray and Light Scattering;* Elsevier/North Holland: New York, 1991, p247.

(23) Nierlich, M.; Williams, C.; Boué, F.; Cotton, J. P.; Daoud, M.; Farnoux, B.; Jannink, G.; Picot, C.; Moan, M.; Wolff, C.; Rinaudo, M.; de Gennes, P. G. *J. Phys. (France)* **1979**, *40*, 701.

(24) Hallberg, R. K.; Dubin, P. L. *J. Phys. Chem. B* **1998**, *102*, 8629−8633/.

(25) Israelachvili, J. *Intermolecular and Surface Forces*; Academic Press: New York, 1992.

(26) Lin, M. Y.; Lindsay, H. M.; Weitz, D. A.; Ball, R. C.; Klein, R.; Meakin, P. *Physical Rev. A* **1990**, *41* (4), 2005−2020.

(27) Kallala, M.; Jullien, R.; Cabane, B. *J. Phys. (Paris) II* **1992**, *2*, 7−25.

(28) Fenistein, D.; Barré, L.; Broseta, D.; Espinat, D.; Livet, A.; J−N. Roux, Scarsella, M. *Langmuir* **1998**, *14*, 1013−1020.

(29) Weitz, D. A.; Huang, J. S.; Lin, M. Y.; Sung, J. *Phys. Rev. Lett.* **1985**, *54* (13), 1416−1419.

(30) Lin, M. Y.; Lindsay, H. M.; Weitz, D. A.; Klein, R.; Ball, R. C.; Meakin, P. *J. Phys.: Condens. Matter* **1990**, *2*, 3093−3113.